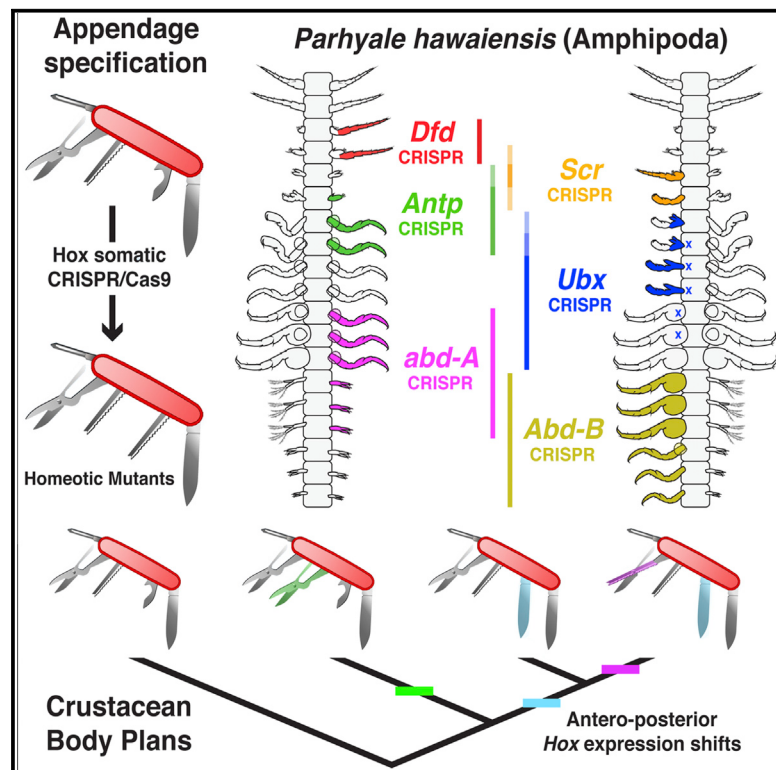


CRISPR/Cas9 Mutagenesis Reveals Versatile Roles of Hox Genes in Crustacean Limb Specification and Evolution

Graphical Abstract



Authors

Arnaud Martin, Julia M. Serano, Erin Jarvis, ..., Carryn A. Barker, Liam C. O'Connell, Nipam H. Patel

Correspondence

nipam@uclink.berkeley.edu

In Brief

Martin et al. analyze the function of six Hox genes in the crustacean amphipod *Parhyale*, using CRISPR/Cas9 mutagenesis and RNAi knockdown. The resulting limb transformations shed light on how each appendage is patterned and how the Hox genes have been used to create several morphological macroevolutionary transitions in the crustacean body plan.

Highlights

- Amphipod crustaceans display a wide array of specialized limbs
- CRISPR mutagenesis and RNAi of Hox genes generate limb transformations
- Limb identity is specified by overlapping domains of Hox expression
- abd-A* expression shifts created evolutionary diversification of the crustacean body

CRISPR/Cas9 Mutagenesis Reveals Versatile Roles of Hox Genes in Crustacean Limb Specification and Evolution

Arnaud Martin,¹ Julia M. Serano,¹ Erin Jarvis,² Heather S. Bruce,¹ Jennifer Wang,² Shagnik Ray,¹ Carryn A. Barker,¹ Liam C. O'Connell,² and Nipam H. Patel^{1,2,*}

¹Department of Molecular Cell Biology, University of California, Berkeley, Berkeley, CA 94720-3200 USA

²Department of Integrative Biology, University of California, Berkeley, Berkeley, CA 94720-3140 USA

*Correspondence: nipam@uclink.berkeley.edu

<http://dx.doi.org/10.1016/j.cub.2015.11.021>

SUMMARY

Crustaceans possess a diverse array of specialized limbs. Although shifts in Hox gene expression domains have been postulated to play a role in generating this limb diversity, little functional data have been provided to understand the precise roles of Hox genes during crustacean development. We used a combination of CRISPR/Cas9-targeted mutagenesis and RNAi knockdown to decipher the function of the six Hox genes expressed in the developing mouth and trunk of the amphipod *Parhyale hawaiensis*. These experimentally manipulated animals display specific and striking homeotic transformations. We found that *abdominal-A* (*abd-A*) and *Abdominal-B* (*Abd-B*) are required for proper posterior patterning, with knockout of *Abd-B* resulting in an animal with thoracic type legs along what would have been an abdomen, and *abd-A* disruption generating a simplified body plan characterized by a loss of specialization in both abdominal and thoracic appendages. In the thorax, *Ubx* is necessary for gill development and for repression of gnathal fate, and *Antp* dictates claw morphology. In the mouth, *Scr* and *Antp* confer the part-gnathal, part-thoracic hybrid identity of the maxilliped, and *Scr* and *Dfd* prevent antennal identity in posterior head segments. Our results allow us to define the role Hox genes play in specifying each appendage type in *Parhyale*, including the modular nature by which some appendages are patterned by Hox gene inputs. In addition, we define how changes in Hox gene expression have generated morphological differences between crustacean species. Finally, we also highlight the utility of CRISPR/Cas9-based somatic mutagenesis in emerging model organisms.

INTRODUCTION

Arthropod appendages have diversified into a remarkable repertoire of specialized morphologies. Crustaceans of the Malacostraca class, such as crabs, lobsters, shrimps, or the emerging model organism *Parhyale hawaiensis*, provide remarkable illustrations of this principle [1, 2], as shown by the extensive morphological and functional diversity of limbs along their antero-posterior (AP) axis (Figure 1A). This extreme specialization provides a Swiss-army knife arrangement of appendages dedicated to perception (antennae), food processing and chewing (mouthparts), prehension (claws or “chelipeds”), walking (legs or “pereopods”), and propulsion (swimmerets or “pleopods”), and at the end of the *Parhyale* abdomen, forked shaped appendages (uropods) are used for anchoring.

In spite of the diversity of forms they can take within a single individual, the limbs along the body axis of a crustacean or insect are serial homologs [4, 5]. Comparative anatomy and gene expression data have revealed that the proximo-distal (PD) limb axis is subdivided into two fundamental territories, a proximal protopod and a distal telopod [6–11]. In crustaceans, the protopod forms the base of this structure and is subdivided into two podomeres, the coxa and the basis (Figure 1B). The basis can be one-branched (uniramous, with an endopod) or two-branched (biramous, with both an endopod and an exite). All crustacean limb appendages are essentially variations on this common theme.

But how do appendages diverge from this basic organization and acquire a specific morphology based on their position along the body? Hox genes play an important role in establishing segmental identity along the AP axis of arthropods and other animals by regulating the transcription of downstream target genes [12, 13]. Furthermore, subtypes of thoracic and abdominal appendages vary in number and position between crustacean species, and comparative studies suggest that spatial shifts of Hox expression have facilitated such rearrangements by modulating a combinatorial code for limb identity [12, 14–20]. For example, comparative analysis of *Ubx* expression across crustacean species suggested that the Hox gene *Ubx* plays a role in defining the transition between feeding and locomotory type appendages in the anterior part of thorax [18]. Functional work in *Parhyale* supported this hypothesis: RNAi-based knockdowns transformed the T2 and T3 clawed appendages into a T1 type feeding limb [21], and misexpression of *Ubx* resulted in ectopic locomotory thoracic appendages in the head [22]. Of note, malacostracan T1 segments deviate from the thoracic leg-like archetype as they bear a maxilliped. Although the maxilliped is part of the T1 segment, it is integrated into the mouth apparatus and shows both gnathal and thoracic features [2]. The *Ubx* RNAi phenotypes

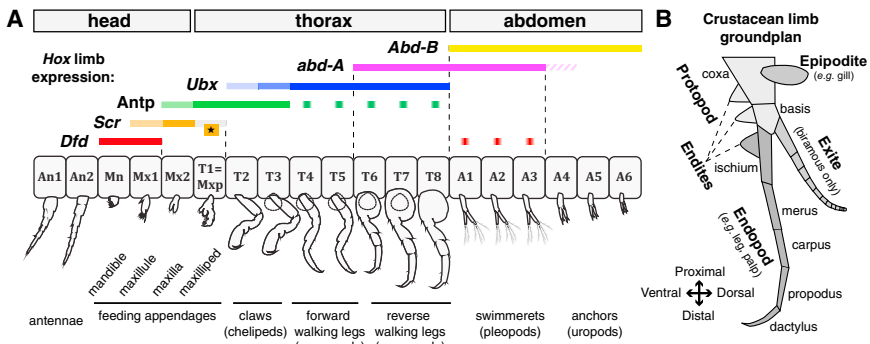


Figure 1. Hox Expression and the Crustacean Limb Body Plan

(A) Summary of Hox expression in *P. hawaiensis* in relationship to specialized segments (after [3]). Faded color bars depict weak expression domains. Green squares indicate neuronal expression of *Antp*. Due to post-translational processing of *Antp* transcripts [3], we show here the domain for *Antp* protein. Red squares indicate mesodermal expression of *Dfd* in the median section of pleopods. The star indicates late, appendage-specific expression of *Scr* in T1/Mxp. The hashed bar indicates transient, weak expression of *abd-A* in A4.

(B) Schematic representation of the crustacean limb groundplan.

(T2 and T3 to a T1 maxilliped) thus suggest that *Ubx* represses gnathal identity in the segments posterior to T1 in *Parhyale*, consistent with the observation that *Ubx* expression is restricted to non-maxilliped segments in every crustacean examined so far [16–18, 21].

Beyond *Ubx*, the potential roles of other Hox genes in determining the positional identity of crustacean limbs, and their evolutionary modification between species, remain unclear due to a lack of functional data. To fill this gap, we used CRISPR/Cas9-targeted mutagenesis and RNAi to systematically interfere with Hox function during the development of *P. hawaiensis* embryos. Gene knockouts of the six Hox genes expressed in the mouth and trunk generated homeotic shifts in limb features. These new results outline the combinatorial logic of a Hox code laying out the segmental identity of crustacean appendages.

RESULTS

CRISPR/Cas9 Loss-of-Function Mutations in G₀ Embryos

RNAi-based approaches have been used for gene expression knockdown during crustacean development [21, 23, 24], and although the approach achieves moderate knockdown of mRNA levels [21], the resulting intermediate phenotypes are still useful. As an alternative, we used CRISPR/Cas9 site-directed mutagenesis targeting the coding sequence of *P. hawaiensis* Hox genes and directly assessed effects in G₀ embryos. Zygotic co-injections of Hox subgenomic RNA (sgRNA) and Cas9 mRNA or protein induced somatic insertion-deletion mutations, including null alleles at targeted sites, (Figures 2A, 2B, and S1). Injected animals can of course be mosaic and contain alleles generated by independent events, but in the case of *Parhyale*, we can use our detailed understanding of the early embryonic lineages to show that CRISPR/Cas9 targeting generates animals in which gene deletion has occurred in large domains, even easily generating unilaterally mutant individuals. To show this, we performed CRISPR injections into one of the two blastomeres after the first zygotic cleavage. Given that this first division separates the left versus right sides for the majority of the body axis [25], we expected to see asymmetric effects. Figure 2C shows the result of such an experiment for *Antp* knockout and illustrates an embryo in which wild-type levels of *Antp* protein are detected in one half, but no protein is detected in the other half, indicating that both *Antp* alleles have been disrupted in all cells on one side

of the embryo. Figure 2D shows an example where we targeted *Ubx* in one of two cells. In this case, the embryo shows wild-type expression of *Ubx* protein on one side and reduced levels on the other side. Of note for this embryo, the T2/3 limb primordia lacked one or two of the seven podomeres observed on the wild-type side, consistent with a transformation of these T2 and T3 appendages toward a T1 (maxilliped) appendage identity, similar to what was seen previously when *Ubx* levels were reduced by RNAi [21].

These results assaying expression after targeting suggest that CRISPR/Cas9 can be used as an efficient tool to generate somatic mutations interfering with gene function during the early embryonic development of *P. hawaiensis* and that the resultant mutant clones are large, most likely due to targeting soon after injection in the zygote. In this respect, it is useful to note that *Parhyale* embryos take 8 hr to go from the one-cell to eight-cell stage. Given this success in knocking out expression, we carried out CRISPR-based loss-of-function experiments targeting the six Hox genes expressed in the mouth and trunk [3]—*Deformed* (*Dfd*), *Sex comb reduced* (*Scr*), *Antp*, *Ubx*, *Abdominal-A* (*abd-A*), and *Abdominal-B* (*Abd-B*)—injecting the one-cell stage to limit mosaicism, and examined the effect of somatic mutagenesis on limb morphology. All but one sgRNA (*abd-A* sgRNA#2; penetrance = 12%) generated limb-specific mutant phenotypes in hatchlings at high efficiency with a penetrance ranging between 25% and 70% (Table S1).

Ubx Represses Mouth Features and Promotes Gill Development

As a proof of principle for generating phenotypes using CRISPR/Cas9, we first replicated the results of previous *Ubx* RNAi injections [21] (Figures 3A and 3B). We obtained embryos in which T2 and T3 were transformed toward T1 (the T1 appendage is a maxilliped and from now on is referred to as T1/Mxp). Importantly, T2/T3 retained a clawed morphology at their distal ends but lost the T2/T3-specific comb bristle, indicating a partial T2/T3-to-T1/Mxp homeosis, which was also what had been observed previously by RNAi. However, we also uncovered additional effects of *Ubx* loss-of-function in T4 and T5. As with transformed T2 and T3 appendages, T4 and T5 also acquired endites with multiple setae at their base, but with the addition of a claw-type morphology at their distal ends (Figures 3A–3C); thus, the transformed T4/T5 displayed aspects of both wild-type T1/Mxp and T2/T3 limbs. Finally, *Ubx* CRISPR resulted in the loss of the five

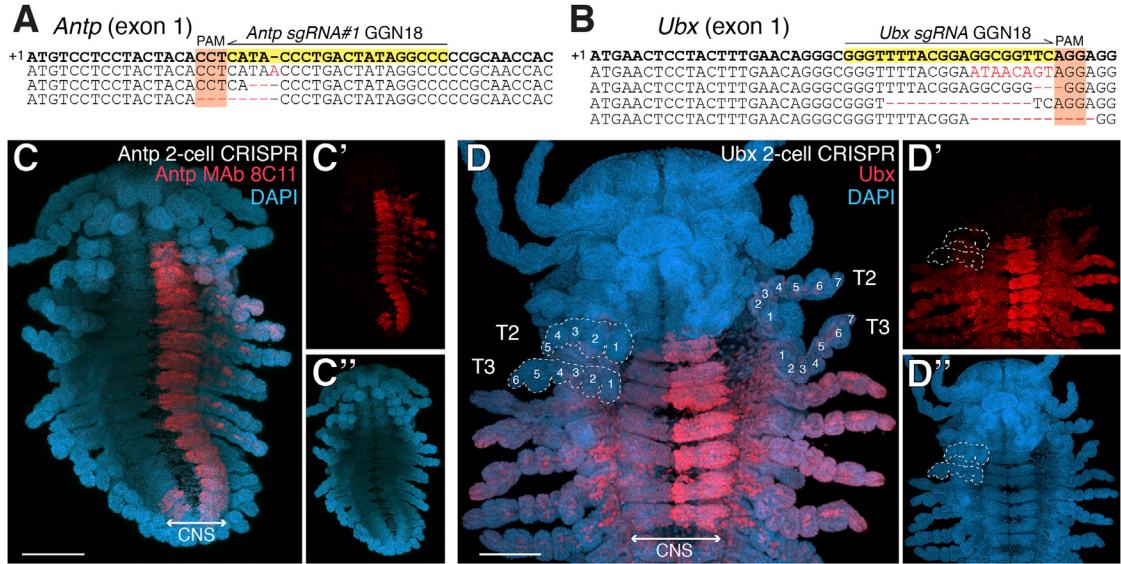


Figure 2. CRISPR Somatic Mutagenesis in *P. hawaiiensis* Embryos

(A and B) Mutant alleles sequenced from single hatchlings around the NGG Protospacer Adjacent Motif (PAM) after zygotic CRISPR injections, targeting *Antp* (A) and *Ubx* (B). Recovered alleles show short, frameshift-inducing indels relative to the wild-type sequences (in bold).

(C) *Antp* immunodetection in a stage 22 embryo after single-cell *Antp* CRISPR injection at the two-cell stage; unilateral expression suggests a complete knockout of *Antp* in the injected lineage.

(D) *Ubx* immunolocalization in a stage-24 embryo, after single-cell CRISPR injection of *Ubx* sgRNA at the two-cell stage. Dotted lines contour T2 and T3 appendages with podomeres numbered. Expression is reduced on one side. Altered morphology of T2 and T3 on the side with reduced expression indicates the transformation of T2 and T3 toward T1/Mxp.

Scale bars, 100 μm. See also Figure S1.

pairs of gills, normally attached at the base of the T3–T7 segments (Figures 3A and 3D). This complements the effects of gain-of-function overexpression of *Ubx*, which induces ectopic gills [22]. Taken together, these results suggest that *Ubx* is necessary for the repression of gnathal identity in the base (proximal podomeres) of T2–T5, and required for gill development in T3–T7.

We interpret the more extreme phenotype seen with CRISPR/Cas9 (with two different sgRNAs) relative to RNAi as the difference between gene knockdown and knockout. The restriction of *Ubx* RNAi effects to T2–T3 suggests these segments are most sensitive to the reduction in the level of *Ubx* expression, and it is worth noting that *Ubx* RNA and protein are expressed at lower levels in these two segments than in T4–T8 in wild-type animals [21]. It is important, however, to consider that CRISPR/Cas9 mutagenesis is also expected to sometimes yield similar partial knockdown effects. In some cases, this may be because the mutant alleles that are generated retain some function or because of the tissue mosaicism inherent to our somatic analysis.

***abd-A* and *Abd-B* Organize the Specialization of Posterior Appendages**

The posterior half of *P. hawaiiensis* shows three pairs of reverse walking legs in T6–T8, three pairs of swimmerets in A1–A3, and three pairs of uropods in A4–A6 (Figure 4A). This anatomical parcellation is reflected at the molecular level by the expression of *abd-A* in the posterior legs and swimmerets (and weakly in the uropod of A4) and by *Abd-B* expression, which extends from the swimmerets to the uropods (Figures 1A and S2). It follows that the partially overlapping expression domains of two Hox

genes creates three Hox states that correlate with morphological differences: (1) *abd-A* in T6–T8, (2) *abd-A* plus *Abd-B* in A1–T3, and (3) *Abd-B* in A4–T6. In the appendages of A1–A3, it appears that all ectodermal cells do co-express *abd-A* and *Abd-B* during limb development (Figure S2). Here we tested the hypothesis that the posterior heteronomy of amphipods is specified by combinatorial Hox expression.

CRISPR somatic mutagenesis of *abd-A* validated this hypothesis and induced three notable limb modifications across its expression domain. First, posterior legs were transformed into anterior legs (T6/8-to-T4/5), as evidenced by their inverted orientation (for instance, with the dactyl pointing backward instead of forward) and by the absence of a large coxa, a characteristic of posterior legs (Figures 4A–4D). Second, the T8 segment acquired an ectopic gill, which is expected from a T8-to-T4/5 transformation (Figures 4B–4D). Third, swimmerets were transformed into uropods (A1/2/3-to-A4/6; Figures 4E–4G), and the A1–A3 abdominal body segments bearing them also transformed toward the A4/5/6 body segments in terms of size and shape, resulting in a severely contracted, narrow abdomen and an aberrant curvature of the body (Figure 4B). Interestingly, *abd-A* loss-of-function phenotypes can be seen as an anteriorization of T6–T8 and as a posteriorization of A1–A3. These results were replicated in CRISPR experiments that used an sgRNA targeting the second exon of *abd-A* (Table S1; Figure S1), thus ruling out off-target effects on limb morphology. In comparison, two independent expression knockdown experiments failed to recreate T6–T8 transformations but succeeded in replicating the effects of *abd-A* CRISPR in the abdomen (Figures 4H and

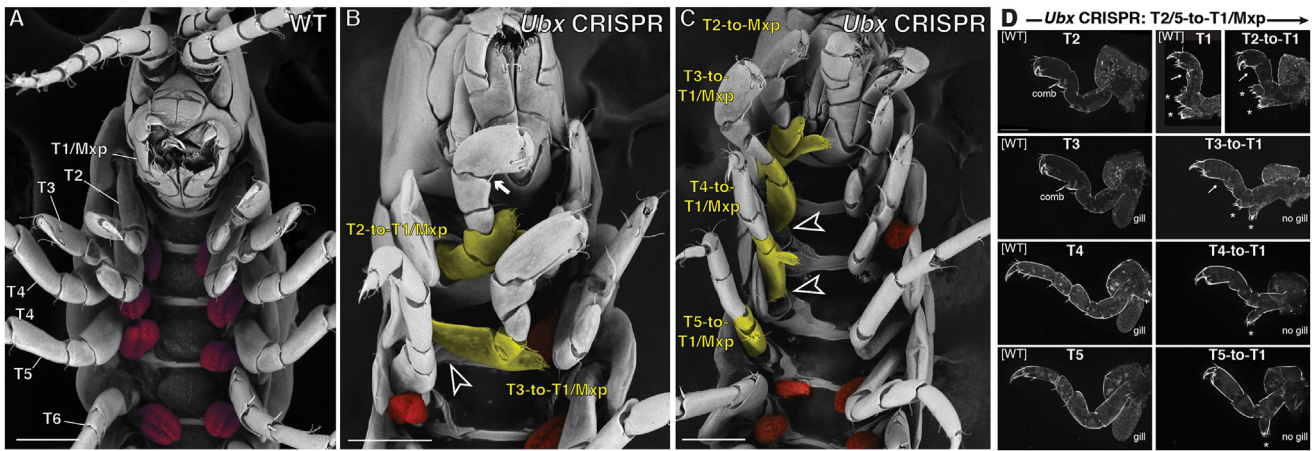


Figure 3. CRISPR Somatic Mutagenesis of *Ubx* Generates Thoracic Limb Anteriorizations and Gill Defects

(A) Ventral scanning electron microscopy (SEM) view of a wild-type hatchling showing thoracic gills (red).
 (B and C) SEM of an *Ubx* CRISPR mosaic mutants; these hatchlings display modified T2–T5 proximal segments (yellow), sometimes displaying ectopic endites. Arrow, comb bristle absent; arrowheads, gills absent (red, wild-type gills).
 (D) Dark-field images of *Ubx* CRISPR limb homeoses. Arrow, comb bristle absent; asterisks, ectopic Mxp-like endites.
 Scale bars, 100 μ m (A–C).

4I). Specifically, the injection of siRNA and two transgenic lines expressing *abd-A* hairpin RNAs under the control of a heatshock promoter [26] all resulted in aberrant swimmerets resembling uropods (A1–A3 transformed toward A4/5/6), characterized by detached pairs of appendages, a curved basis, and a failure to develop propulsive setae. This suggests again the importance of Hox expression levels—in this case, A1–A3 are more sensitive to lowering *abd-A* expression than are T6–T8.

In accordance with its pan-abdominal expression, *Abd-B* CRISPR transformed both swimmerets and uropods into walking legs (Figures 4J–4M), culminating in a densely packed array of legs as seen across one side of the entire abdomen in Figure 4K. The induced legs displayed a large (T8-like) coxa in the A1–A3 segments and a narrow coxa characteristic of anterior legs (T4/5-like) in the A4–A6 segments. We deduce that disruption of *Abd-B* transforms A1–A3 toward T6/7/8 and A4–A6 toward T4/5 in *abd-A*-positive and *abd-A*-weak/negative domains, respectively. In extreme cases, transformed legs in the *abd-A*-weak A4 segment showed an ectopic gill reminiscent of the *abd-A* CRISPR T8-to-T4/5 transformation (Figure 4M). It will be interesting to test whether *Ubx* expression extends posteriorly into the abdomen upon *Abd-B* knockout, which could explain these gill acquisitions.

Abd-B RNAi injections showed a similar, but less severe effect: both swimmerets and uropods underwent a biramous-to-uniramous transition, with most swimming segments taking a walking-leg morphology (Figures 4N–4Q). Although these incomplete transformations are most likely due to a limitation of the knockdown approach, *Abd-B* RNAi succeeded in forming fully differentiated reverse walking legs in the first abdominal segment (A1-to-T8). Thus, several lines of evidence show that *Abd-B* is necessary for the maintenance of abdominal limb identity and promotes biramous morphology.

***Antp* Functions in Claw Specification**

Amphipod thoracic legs are subdivided into three types—prehensile claw-like chelipeds (T2–T3), forward-walking legs

(T4–T5), and reverse-walking legs (T6–T8). While *abd-A* directs the differentiation of reverse- versus forward-walking legs, *Ubx* disruption did not explain the genetic demarcation between claws and walking legs in the anterior thorax. This functional subdivision could depend on *Antp*, which is expressed in clawed segments, but not in developing walking legs [3]. *Antp* CRISPR validated this hypothesis and yielded cheliped-to-forward-walking-leg transformations (T2/3-to-T4/5), as evidenced by the narrow shape of the propodus segment and by the loss of T2/3-specific comb bristles involved in grooming (Figures 5A–5D). Modified chelipeds failed to acquire normal segmentation and retained a fused ischium-merus (Figure 5C). In wild-type animals, gills are only observed in T3–T7 segments, but remarkably, T2 transformed limbs also displayed an ectopic gill indicative of a more posterior specification (T2-to-T4/5). This anatomical gain provides additional evidence for a homeotic effect of *Antp* somatic mutagenesis on the entire appendage. As these results were obtained for two distinct sgRNAs of comparable penetrance, we have ruled out off-target effects of *Antp* CRISPR on limb morphology and conclude that *Antp* is required for the specification of chelipeds.

Complementary Effects of *Antp* and *Scr* in Maxillipeds

In contrast with the thorax and abdomen, arthropod mouthparts generally show a sequential heteronomy where all consecutive segments are distinct and differ from each other, without repetition. In the next two sections, we explore how sequential expression of Hox genes might explain the differentiation of the amphipod mouth apparatus. In addition to its effects on chelipeds, *Antp* CRISPR also resulted in visible defects in maxillipeds. *Antp* mutant jaws showed T1/Mxp-to-Mx1 transformations, as revealed by the acquisition of Mx1-specific serrated setal teeth on the basis endite and by a narrow coxal endite, topped by two long simple setae (Figures 5A–5B and 5E–5G). In contrast, wild-type T1/Mxp endites both resemble the Mx2 condition (Figure 5H). Disruption of *Antp* also showed graded effects of the T1/Mxp endopods, the more distal part of the limb. In the

milder forms, the T1/Mxp endopod regressed into a palp of bulging aspect, due to an abnormally narrow attachment site on the basis article (Figure 5G). These transformed limbs display three endites instead of two, due to the maintenance of the ischium and basis endites with an ectopic and prominent, Mx1-like coxal endite. In more extreme forms, the endopod was missing from the T1/Mxp-to-Mx1 transformed limb (Figure 5I). Altogether, these results underline the dual role of *Antp* in maxilliped development, as it selects the identity of the proximal domain while also being required for palp growth in the distal domain.

Scr expression (Mx1-T1/Mxp) overlaps with *Antp* (Mx2-T3) in the mouth, and hatchlings that were injected with *Scr* CRISPR showed a mild to severe disorganization of the jaw due to an imperfect interlocking of the modified mouthparts. Upon closer inspection, *Scr* mosaic mutants revealed maxilliped-to-cheliped transformations (T1/Mxp-to-T2/3), with the distal palp acquiring both a T2/3-specific comb bristle and the morphology of a pre-hensile claw, characterized by an enlarged propodus and an opposing dactyl (Figures 6A–6C). In the proximal domain, T1/Mxp endites regressed upon *Scr* loss of function, consistent with a conversion of this appendage toward a thoracic identity.

In summary, both the CRISPR phenotypes of both *Antp* and *Scr* mutants reveal a modular, composite organization of the maxilliped, with dual effects on the proximal and distal domains. *Scr* functions as a determinant of the gnathal identity of the protopod, and *Antp* is necessary for preventing Mx1-like morphology in this limb domain. Conversely, in the T1/Mxp endopod, *Scr* inhibits the posterior claw-like morphology of the palp, and *Antp* is required for endopod presence. The antagonistic roles of these genes may thus explain the hybrid nature of maxillipeds, by conferring a combination of thoracic (presence of an endopodal extension) and gnathal (sensory endites and clawless palp) features.

Conserved Functions of *Scr* and *Dfd* in Mouth Patterning

The mandible (Mn), maxillule (Mx1), and maxillae (Mx2) are consecutive mouth appendages involved in food processing along with the more posterior T1 maxilliped. Mn or Mx1 palps are common among other amphipods, but in *P. hawaiiensis*, a residual palp is apparent on Mx1 only and the three appendages thus appear to repress endopod development. CRISPR-induced mutagenesis of both *Scr* and *Dfd* revealed that these genes control different aspects of the regional identity of these segments on the PD axis.

Wild-type Mx2 have two lobes with simple setae (the coxa and basis endites). Although this appendage is thus devoid of an endopod, both RNAi- and CRISPR-based loss of function of *Scr* activated endopodal growth (Figures 6D and 6E). *Scr* CRISPR individuals showed a gradual series of Mx2 modifications, starting with the presence of an ectopic endopod and the acquisition of serrated setae characteristic of the Mx1 segment on the endites (Mx2-to-Mx1). In the most extremes cases, the endites regressed, and an antenna-like endopod protruded from the side of the mouth (Mx2-to-An). *Scr* RNAi resulted in less dramatic, but still striking, Mx2 phenotypes with the formation of ectopic but incomplete endopods, and the acquisition of an additional endite-bearing ischium—a condition that exists in the maxilliped of *Parhyale* and other amphipods [2]. This transformation of Mx2 to T1/Mxp

(Figure 6D) is consistent with the phenotype seen when low levels of *Ubx* misexpression cause a reduction in the levels of *Scr* [22]. *Scr* RNAi had no effect on the Mx2 proximal domain or on Mxp, suggesting a lower expressivity than *Scr* CRISPR.

Like *Scr* in Mx2, *Dfd* CRISPR promoted endopodal development in Mn and Mx1 (Figures 6F–6I). In *Dfd* mutants, the Mx1 vestigial endopod developed into a segmented antenna, whereas the proximal domain retained an Mx1 identity (partial Mx1-to-An). *Dfd* CRISPR also induced the formation of an ectopic endopod on Mn, resulting in a dislocated mandible protruding from the mouth apparatus or culminating in the formation of a short and segmented antennal primordium (Mn-to-An).

Taken together, these results show that *Scr/Dfd* loss-of-function experiments both induce antenna-like appendages in the mouth. Similar phenotypes have been observed in homologous segments upon *Scr/Dfd* knockdown in hemipterans and coleopterans, suggesting an evolutionarily conserved role in the maintenance of gnathal identity between insects and crustaceans [27–31]. In the proximal domain of mouth appendages, *Scr* in particular patterns the setulation of Mx2/T1 endites, whereas *Dfd* prevents spurious Mx1 morphology in the Mx2 segment. We conclude that in addition to an ancestral function in the distal repression of antennal fate, the sequential expression of *Scr* and *Dfd* in the mouth also contributes to the heteronomy of this body region via modular effects along the limb PD axis.

DISCUSSION

Using CRISPR for Somatic Analyses of Gene Function

The recent development and apparent universality of CRISPR/Cas9 genome editing [32] allowed us to analyze the function of the six Hox genes expressed in the mouth and trunk of *P. hawaiiensis*, an emerging model organism (Figures 7A and 7B). We used zygotic injections to generate DNA lesions in the soma, without attempting stable germline transformation. Here we discuss this strategy and the extent to which it could foster discovery in analogous experimental systems.

Cost

We generated ready-to-inject samples in 2–3 days and at low cost (less than \$80 per target in reagents).

Penetrance

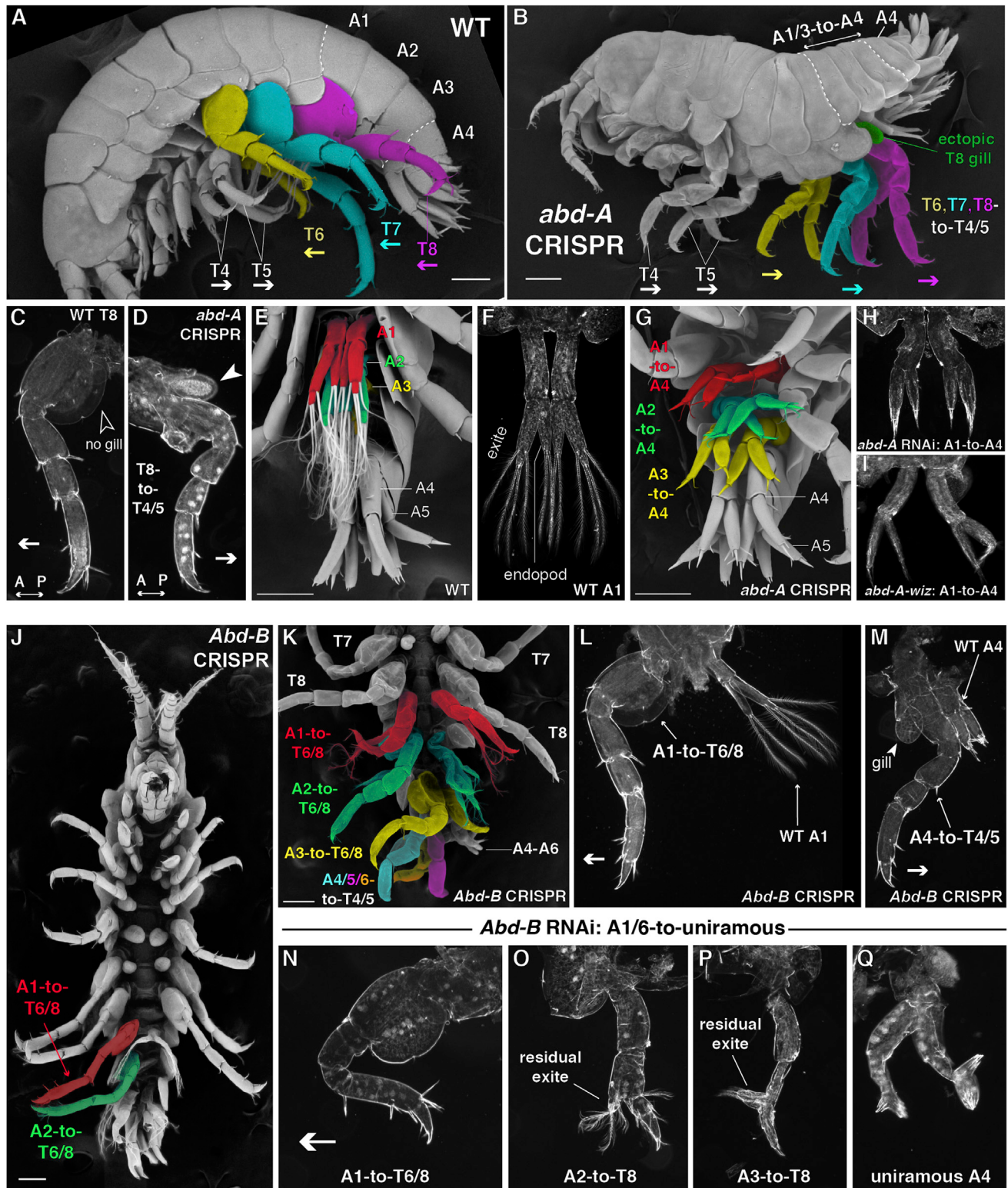
CRISPR/Cas9 somatic loss-of-function experiments generated homeotic phenotypes at high frequency for eight out of the nine sgRNAs that were assessed (Table S1). The lower efficiency of *abd-A* sgRNA#2 (12% penetrance) may be explained by the fact it was the only sgRNA targeting a short second exon (Figure S1), which could be subject to splicing.

Expressivity

In all our comparisons (*Scr*, *Ubx*, *abd-A*, and *Abd-B*), CRISPR showed more marked effects than siRNA injections, with an increased degree of transformation. These limitations of RNAi are most likely due to incomplete mRNA knockdown in *Parhyale* [21], although clearly the combination of CRISPR and RNAi data was useful in revealing the relative sensitivity of different segments to Hox gene perturbation.

Reproducibility and Target Specificity

Although it would be difficult to assess the target specificity of CRISPR in our model system, we sought to test the reproducibility of limb transformation phenotypes using non-overlapping

**Figure 4. abd-A and Abd-B Pattern Functional Subdivisions in Thoracic and Abdominal Appendages**

(A and B) Lateral SEM views of wild-type (A) and *abd-A* CRISPR-injected (B) *Parhyale* hatchlings; *abd-A* CRISPR results in leg homonomy, with anteriorization of the reverse-walking morphology in T6–T8 and ectopic gills in normally gill-less T8. Mutant abdomens curl upward due to A1–A3 posteriorization.

(C and D) Dark-field images of dissected wild-type (C) and *abd-A* mutant (D) T8, with reversed polarity in the antero-posterior (AP) axis.

(E and F) Ventral views of wild-type pleopods (A1–A3 swimmerets), characterized by a biramous morphology terminated by long setae.

(legend continued on next page)

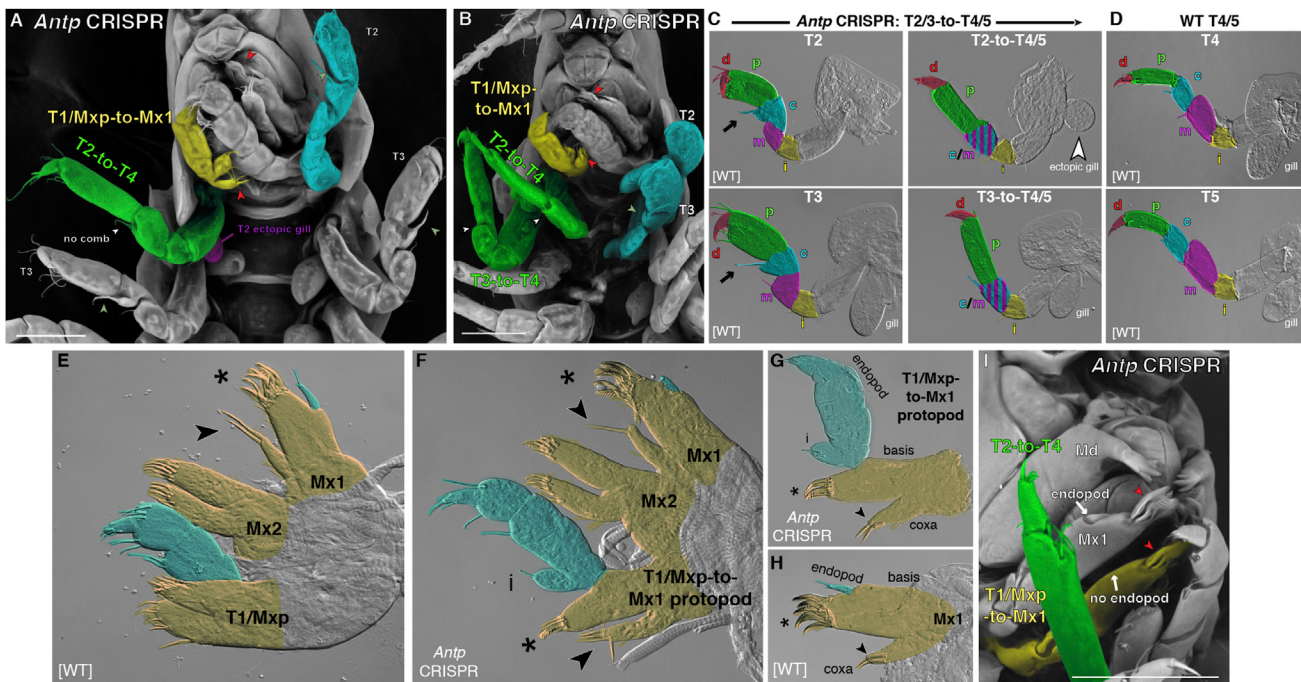


Figure 5. *Antp* Is Required for Limb Specialization in the Anterior Thorax

(A) Ventral SEM view of a unilateral mutant hatching obtained by *Antp* CRISPR. The mouth is dislocated due to an incomplete T1/Mxp-to-Mx1 transformation (yellow), bearing Mx1-specific setal teeth (red arrowheads). The transformed T2 limb (green) lacks a normal claw morphology and the T2/3 specific comb bristle (white arrowheads, absent; green, wild-type) and shows an ectopic gill (purple).

(B) Another example of a unilateral *Antp* CRISPR mutant, notably showing a T2/3-to-walking-leg transformation (green).

(C) Differential interference contrast (DIC) imaging of T2/3 limbs transformed by *Antp* CRISPR, with endopod podomeres false colored. Arrow, comb bristle (absent in mutants); d, dactylus; p, propodus; c, carpus; m, merus; i, ischium.

(D) Wild-type T4 and T5 forward-walking legs.

(E–H) Detailed morphology of the maxillary apparatus in wild-types (E and H) and *Antp* CRISPR mutants (F and G). Blue, endopods; yellow, protopods; asterisk, Mx1-basis-specific setal teeth; arrowhead, Mx1-coxa-specific endite.

(I) Unilateral *Antp* CRISPR mutant showing a T1/Mxp-to-Mx1 transformation with a complete ablation of the endopod.

Scale bars, 100 μm (A, B, and I).

sgRNAs (for *Dfd*, *Scr*, *Antp*, and *abd-A*). In these four cases, mutant phenotypes were equivalent regardless of the 19–20 bp nucleotides targeted. RNAi phenotypes obtained for *Ubx*, *abd-A*, and *Abd-B* were also consistent with the effects of CRISPR mutagenesis in these genes. These results provide independent replications and rule out off-target effects of CRISPR/Cas9 somatic mutagenesis on limb morphology.

Mosaicism

A caveat of somatic mutagenesis is linked to the random occurrence of DNA cleavage in post-zygotic stages [34]. We have seen

that CRISPR injections have the potential to generate bi-allelic knockouts that spread to large sections of the injected individual by clonal inheritance (Figure 2C). For any given transformed animal, the distribution of mutant cells and their respective allelic dosage are unknown (Figure 2D). That said, the resulting mosaicism can be advantageous for several reasons. First, unilateral mutant phenotypes can be directly compared to a wild-type state within the same animal, providing an internal control. Second, for pleiotropic genes involved in several processes across development, mosaicism may increase the rate of surviving

(G) Ventral view of an *abd-A* CRISPR somatic mutant. The A1–A3 pleopods are disjointed and acquire a more posterior, uropod-like morphology lacking long setae.

(H) Pleopod-to-uropod transformation obtained after zygotic injection of *abd-A* siRNA.

(I) Pleopod-to-uropod transformation obtained in the *hsp70-abd-A-wiz* transgenic line.

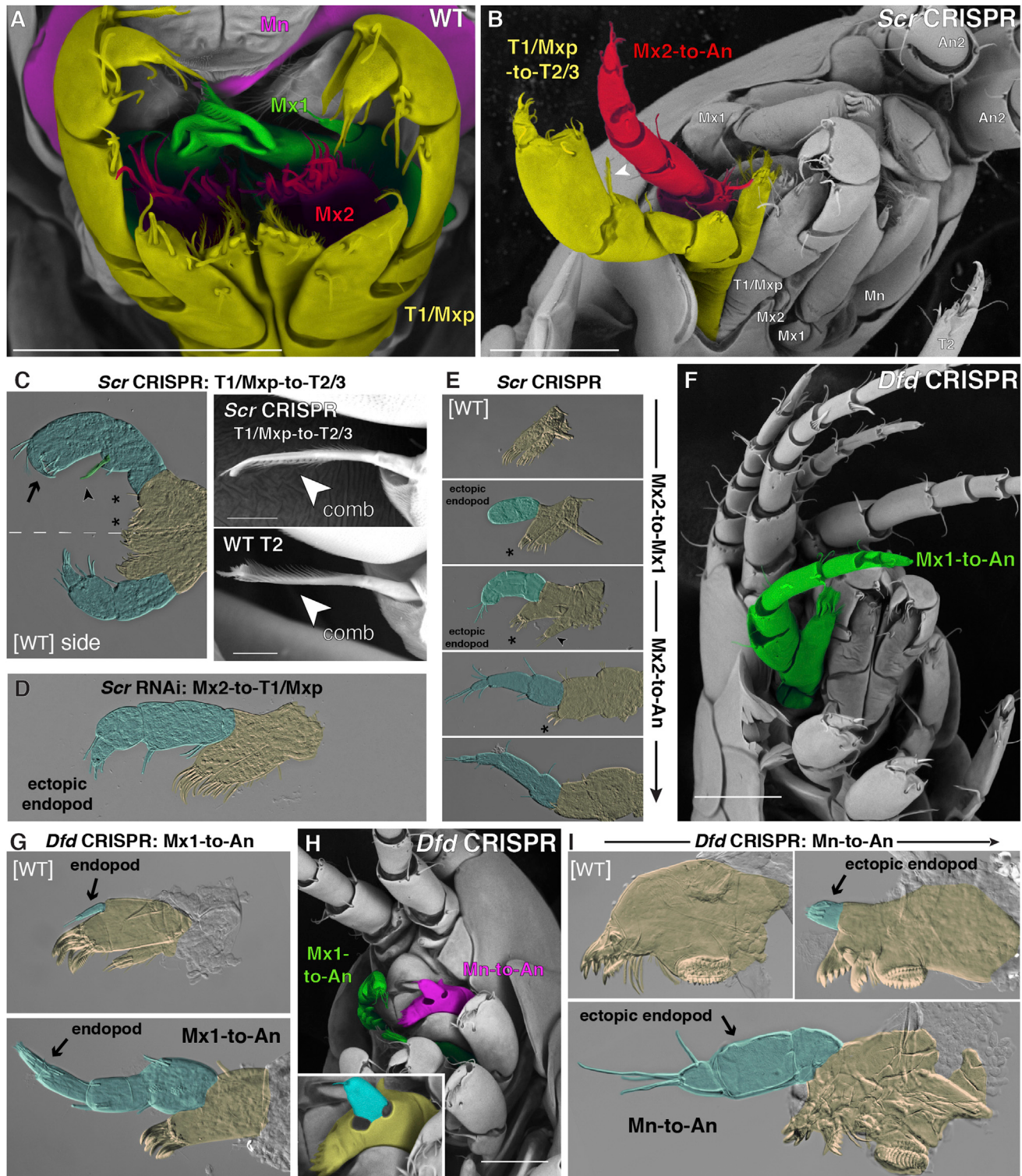
(J and K) Ventral views of *Abd-B* CRISPR mosaic mutant hatchlings. Abdominal segments show gradual transitions toward a leg-like, uniramous morphology, including complete A1/3-to-T8 and A4/6-to-T4/5 transformations.

(L) Dorsal view of the flattened appendages of the A1 segment of an *Abd-B* CRISPR mosaic mutant with a unilateral transformation of a pleopod into a posterior leg with large coxa (A1-to-T8).

(M) Dorsal view of an *Abd-B* CRISPR mosaic mutant with a unilateral transformation of a uropod into a gilled anterior leg (A4-to-T4/5).

(N–Q) Variable partial transformations of the biramous A1–A4 limb toward a uniramous morphology after *Abd-B* RNAi zygotic injections, including complete transformations into reverse-walking (T8-like) legs (N). Effects similar to those in (Q) were obtained for A5–A6.

See also Figure S2.

**Figure 6. Scr and Dfd Maintain Gnathal Features in Mouth Appendages**

(A) Ventral SEM view of a wild-type mouth apparatus.

(B) Mouth identity defects in a unilateral Scr CRISPR mutant. Arrowhead, T2/3-specific comb bristle.

(C) Ventral view of a dissected, unilaterally transformed pair of Scr CRISPR maxillipeds. Arrow, T2/3-like claw morphology of the dactylus/propodus; arrowhead, T2/3-specific comb bristle; asterisk, regressed T1/Mxp endites.

(D) Effect of Scr RNAi on Mx2, with growth of an ectopic endopod (blue).

(legend continued on next page)

“escapers” by randomizing the distribution of mutant clones. Last, mosaicism can generate phenotypic series that are biologically informative. In our case, this was true for *Scr* CRISPR, in which intermediate (Mx2-to-Mx1) and severe homeosis (Mx2-to-An) suggested two distinct functions of this gene in the maxilla segment.

Overall, we encourage the use of CRISPR/Cas9 somatic mutagenesis for the rapid analysis of gene function in emerging model organisms with injectable eggs, complementing the already widespread use of RNAi. This should notably facilitate the systematic study of Hox gene function across a broad sample of arthropods, drawing the promise of an extended understanding of segmental and serial homolog evolution. For instance, CRISPR has been successfully carried out in the brachiopod *Daphnia magna* [35]. Hox mutagenesis in this species would extend existing gene expression analyses [36] and could yield important comparative insights into the macroevolution of crustaceans.

Hox Expression Shifts and the Evolution of the Crustacean Trunk

CRISPR mosaic mutants reveal that *abd-A* and *Abd-B* expression domains determine segmental identity in the thorax and abdomen. This combinatorial model sheds light into the evolution of abdominal appendages. In four malacostracans, *Procambarus*, *Porcellio*, *Mysidium*, and *Mysidopsis*, *abd-A* is expressed in the first five abdominal segments (containing pleopods), but not in the uropods of A6, the sixth and final abdominal segment [4, 16, 17] (summarized in Figure 7C). To replicate these previous results, we profiled the distribution of the *Ubx*/*abd-A* proteins using the cross-reactive FP6.87 monoclonal antibody [37, 38] in *Procambarus fallax* (Decapoda) and *Mysidium columbiae* (Mysida) embryos. As previously reported, we found that the A6 segment of both decapods and mysids lacked *abd-A*, correlating with the presence of a pair of uropods rather than pleopods on A6 (Figures 7D–7F). In other words, *abd-A*-weak abdominal segments are always associated with a uropod identity. The three pleopod plus three uropod segment arrangement is unique to amphipods and may have been caused by an amphipod-specific loss of *abd-A* expression in A4–A5 (Figure 7H).

CRISPR somatic knockouts approximate this evolutionary scenario, as the experimental disruption of *abd-A* resulted in pleopod-to-uropod transformations, which validates a functional link between *abd-A* deployment and pleopod/uropod ratio. The posteriorization of the A1–A3 domain also suggests that *abd-A* works in conjunction with the overlapping expression of *Abd-B* in this region to establish pleopod identity. This is a new exception to the “posterior prevalence rule” [39], which would have predicted an absence of *abd-A* function in cells co-expressing the more posterior Hox gene *Abd-B*. Both comparative and functional data thus suggest that spatial shifts of *abd-A* deployment modulate the number of *abd-A*-negative uropods,

explaining divergent arrangements of abdominal appendages in crustaceans.

Amphipods are also characterized by the presence of two types of legs (“amphi-poda,” gr. “different foot”), in contrast with isopods, which possess a single type of walking-leg morphology. In our amphipod model organism, *abd-A* mutagenesis replaced the reverse-walking legs with additional forward-walking legs, resulting in an isopod-like configuration. Accordingly, *abd-A* is not expressed in the legs of an isopod [16], suggesting that disruption of *abd-A* in the amphipod thorax effectively recapitulated the isopod state (Figure 7H). Given the central role that Hox genes play in determining arthropod segment identity, evolutionary shifts in Hox expression domains may provide a recurring strategy to generate diverse arrangements of specialized limb types [12, 40].

Hox Functions in the Modular Evolution of Maxillipedes

Our model for how shifts in *abd-A* and *Antp* expression have accompanied morphological evolution of the crustacean body plan is similar to the proposed role of *Ubx* in generating diversity in the number of crustacean maxillipedes [18]. Crustaceans exhibit anywhere from zero to three pairs of maxillipedes, and the number of maxillipedes correlates with the position of the anterior boundary of *Ubx* expression; in other words, appendages of the anterior thorax that lack *Ubx* expression become maxillipedes, whereas those that express *Ubx* become claws or legs [18, 21, 22].

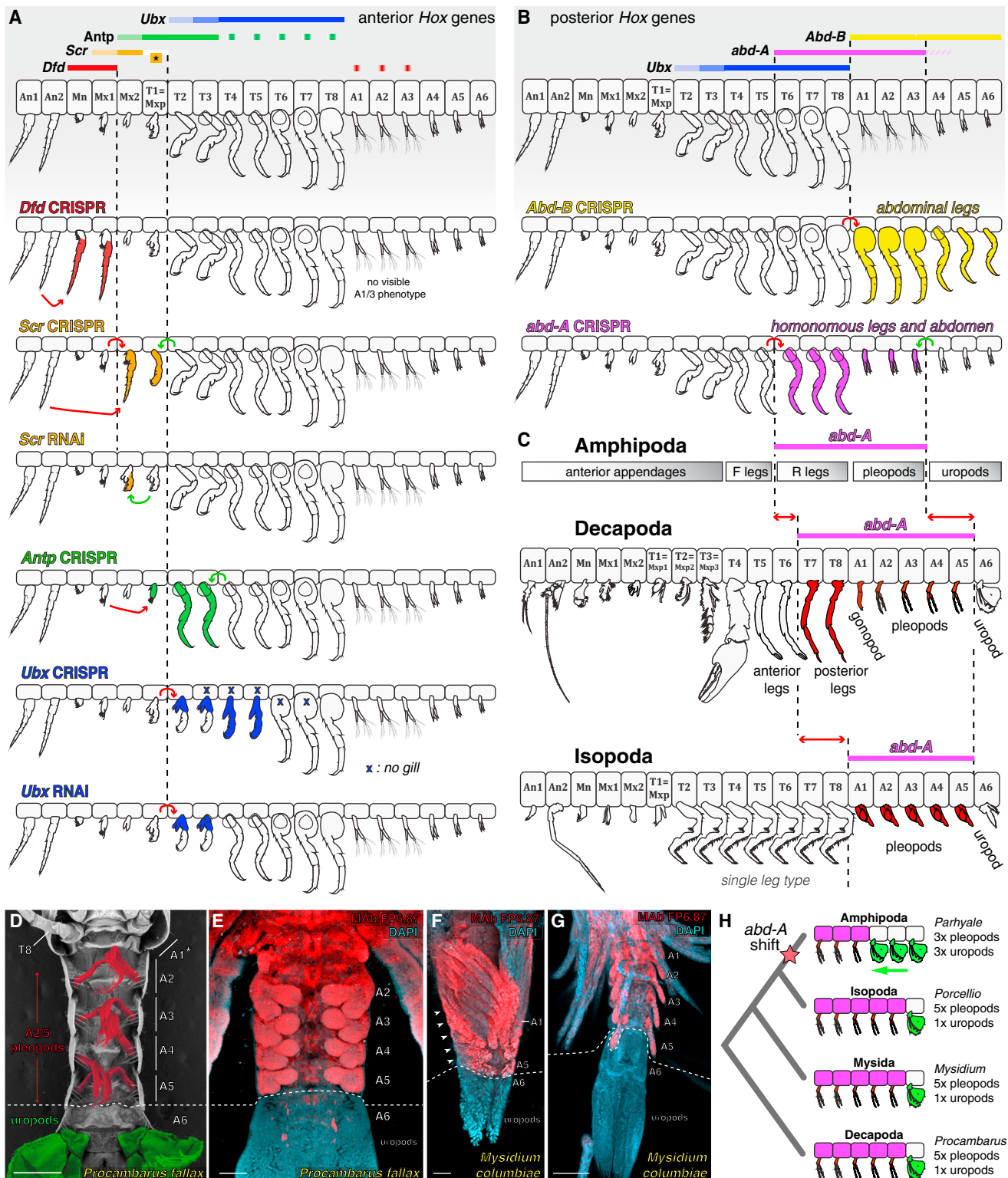
Although *Ubx* represses gnathal identity the thorax, it does not explain the “chimeric”—both gnathal and thoracic—identity of the maxilliped [41], a composite identity that relies on the selector activities of more anterior Hox genes. Indeed, we found that interfering with Hox gene functions triggered modular effects on feeding appendages, with endite-bearing articles requiring *Scr*, the maxilliped endopod requiring *Antp*, and either *Scr* or *Dfd* repressing antenna-like endopods in maxillae (Mx1) and maxillules (Mx2). The compartmented functions of these consecutive genes may contribute to the robust establishment of differentiated morphologies in adjacent mouth segments, and they also shed light on the composite nature of maxillipedes. Indeed, *Scr* and *Antp* show dual functions that are complementary in each section of T1/Mxp. In the proximal section, *Scr* is necessary for the growth of endites while *Antp* provides positional identity. The Mxp distal domain shows a reverse pattern, with a requirement of *Antp* for palp growth, while *Scr* provides positional identity. The ability of Hox genes to perform different functions along the PD axis has been linked to the Hox co-factors *Homothorax* (*Hth*) and *Extradenticle* (*Exd*) in insects [31, 42–51]. Because *Exd* and *Hth* expression mark proximal limb domains in the crustacean limb [6, 7, 10, 11], *Exd/Hth/Hox* protein interactions could explain the differential effects of genes such as *Antp*, *Scr*, and *Dfd* in the proximal versus distal domains of the *Parhyale* feeding segments. Combinations of Hox genes and proximal co-factors may thus form a molecular canvas for

(E) Spectrum of effects of *Scr* CRISPR on Mx2, with growth of an ectopic endopod (blue), acquisition of Mx1 protopod identity (asterisk, Mx1-specific setal teeth on basis endite; arrowhead, Mx1-specific coxal endite), and in most marked phenotypes, acquisition of an antenna-like morphology.

(F and G) Transformation of the Mx1-endopod into an antennal morphology (green) in *Dfd* CRISPR mosaic mutant hatchlings.

(H and I) Acquisition of an ectopic antenna-like endopod (blue) in the Mn appendage after *Dfd* CRISPR.

Scale bars, 100 μm (A–B, F, and H) and 10 μm (C).

**Figure 7. The Control of Crustacean Limb Identity by Hox Genes**

(A and B) Summary of all known Hox loss-of-function phenotypes in *P. hawaiensis*. Arrows indicate the directionality of the homeosis (red, anteriorization; green, posteriorization); dotted lines indicate gills

(C) AP shifts in *abd-A* expression recapitulate the evolution of limb-type subdivision in both thoracic legs and abdominal appendages (this study) [16, 17, 26]. Notice that *abd-A* loss of function triggers homeotic shift of opposite directions on each side of its expression domain in *P. hawaiensis* (B). F legs, forward-walking legs; R legs, reverse-walking legs.

(legend continued on next page)

the modular evolution of crustacean limbs, as reflected by the chimeric organization of crustacean maxillipeds.

Arthropod appendages are often used as an example of dramatic evolutionary diversification of form and function, and there are numerous examples of correlations between gene expression and differing morphologies between species. In some cases, these correlations have included expression changes in Hox genes, and other studies have implicated evolutionary shifts in Hox gene targets. Our functional studies can now point to the shifting domains of Hox genes as part of the basis for crustacean body-plan evolution, but there is no doubt that this will only be part of the explanation.

EXPERIMENTAL PROCEDURES

Detailed experimental procedures are presented in the [Supplemental Experimental Procedures](#).

CRISPR/Cas9 Somatic Mutagenesis

Preparation of Cas9 mRNA followed a published procedure [52], with the exception that we used the *pCasX* plasmid linearized with *Acc65I* as a template for T7 transcription [53]. For sgRNA design, we used the ZIFIT Targeter webtool [54] to scan for GGN_{17–18}[NGG] motifs in Hox gene open reading frames and generated oligonucleotides integrating target specific GGN_{17–18} into a tracrRNA sequence ([Supplemental Experimental Procedures](#)). PCR assembly of the DNA templates, in vitro transcription, and purification of sgRNAs followed a previously published protocol [52]. Cas9 mRNA and sgRNA were mixed in a 1:2 molar ratio, purified, suspended in water, and stored at –80°C until injection. Injection mixes based on Cas9 protein consisted of aqueous re-suspensions of 333 ng/μl recombinant Cas9-NLS protein (PNA Bio, catalog number CP01), 200 ng/μl sgRNA, and 0.05% phenol red dye for injection visualization.

RNA Interference

Stealth siRNA duplexes were designed using the BLOCK-IT RNAi Designer tool (Thermo Fischer Scientific) in non-conserved coding regions of the *Parhyale Scr*, *abd-A*, and *Abd-B* transcripts [3]. The *abd-A-wiz* construct was generated by directional cloning of 544nt *abd-A* fragments into a modified version of the *pWIZ* vector [26]. The resulting construct, consisting of the *abd-A* fragment in opposite orientations on either side of the *Drosophila white* intron, was then placed downstream of the *Parhyale hsp70* promoter within a *pMinos* transformation vector, and germline transformation was carried out as previously described [55, 56]. Embryos from females that carried the *hsp70-abd-A-wiz* transgene were isolated and subjected to daily, 1-hr-long heat shocks beginning around stage 14 (i.e., just before the onset of endogenous *abd-A* expression) and continuing until hatching. Two independent transgenic lines were established, and both yielded similar results.

Injections and Imaging

Embryo injection followed a published protocol [57]. For CRISPR somatic mutagenesis, approximately 40–60 picoliters of 400–600 ng/μl Cas9 mRNA/sgRNA mixture were injected into one-cell embryos. For RNAi, approximately 20–40 picoliters of 200 μM siRNAs were injected into one-cell embryos or both cells of two-cell embryos. For examination of limb phenotypes, *P. hawaiensis* hatchlings were fixed for 2 hr in 3.7% formaldehyde, and appendages were removed individually, mounted in 70% glycerol, and visualized with dark-field and DIC optics. For SEM, *P. hawaiensis* and *P. fallax* hatchlings were fixed for

2 hr in 3.7% formaldehyde, dehydrated via an ethanol series prior to critical point drying, and examined on a Hitachi TM-1000. *M. columbiae* specimens used for SEM were obtained from a stock of adults that had been fixed and stored in MeOH. SEM images were false-colored using the “Darken” and “Soft Light” layer functions of Adobe Photoshop.

SUPPLEMENTAL INFORMATION

Supplemental Information includes Supplemental Experimental Procedures, two figures, and one table and can be found with this article online at <http://dx.doi.org/10.1016/j.cub.2015.11.021>.

AUTHOR CONTRIBUTIONS

N.H.P., A.M., and J.M.S. conceived the project. A.M., E.J., J.W., H.S.B., and S.R. performed CRISPR/Cas9 mutagenesis and analysis. J.M.S. and C.A.B. carried out RNAi. E.J. and L.C.O. performed antibody and *in situ* analysis. A.M., N.H.P., and J.M.S. wrote the manuscript with input from all co-authors.

ACKNOWLEDGMENTS

We thank Ira Blitz and Arul Subramanian at University of California, Irvine for sharing the *pCasX* plasmid, the personnel of the Electron Microscope Lab at University of California, Berkeley for assistance with SEM, and three reviewers for insightful comments on the manuscript. This work was supported by NSF grant IOS-1257379 to N.H.P.

Received: September 16, 2015

Revised: November 9, 2015

Accepted: November 9, 2015

Published: December 10, 2015

REFERENCES

- Brusca, R.C., and Brusca, G.J. (2003). *Invertebrates*, Second Edition (Sinauer Associates).
- Schram, F.R. (1986). *Crustacea* (Oxford University Press).
- Serano, J.M., Martin, A., Liubicich, D.M., Jarvis, E., Bruce, H.S., La, K., Browne, W.E., Grimwood, J., and Patel, N.H. (2015). Comprehensive analysis of Hox gene expression in the amphipod crustacean *Parhyale hawaiensis*. *Dev. Biol.* Published online November 10, 2015. <http://dx.doi.org/10.1016/j.ydbio.2015.10.029>.
- Panganiban, G., Sebring, A., Nagy, L., and Carroll, S. (1995). The development of crustacean limbs and the evolution of arthropods. *Science* 270, 1363–1366.
- Williams, T.A. (2003). The evolution and development of crustacean limbs: an analysis of limb homologies. In *Evolutionary Developmental Biology of Crustacea, Crustacean Issues*, G. Scholtz, ed. (CRC Press), p. 220.
- Giorgianni, M.W., and Patel, N.H. (2004). Patterning of the branched head appendages in *Schistocerca americana* and *Tribolium castaneum*. *Evol. Dev.* 6, 402–410.
- González-Crespo, S., and Morata, G. (1996). Genetic evidence for the subdivision of the arthropod limb into coxopodite and telopodite. *Development* 122, 3921–3928.
- Jockusch, E.L., Williams, T.A., and Nagy, L.M. (2004). The evolution of patterning of serially homologous appendages in insects. *Dev. Genes Evol.* 214, 324–338.

(D) Ventral SEM view of the abdominal appendages of a decapod crayfish hatchling, with only the A6 segment bearing a uropod. Asterisk, A1 appears to be limbless in hatchlings, but males develop a gonopod (modified pleopod involved in reproduction) at the juvenile stages.

(E) FP6.87 staining of a crayfish embryonic abdomen (red); staining is absent from A6 and uniform in A2–A5 limb primordia.

(F and G) FP6.87 staining of the embryonic abdomen of a mysid shrimp at successive stages (red); staining is absent from the uropod-bearing A6 segment and uniform in A1–A5 pleopod primordia.

(H) Modification of abdominal limb distribution in Amphipoda (tree topology after [33]).

Scale bars, 500 μm (D and E) and 100 μm (F and G). See also [Table S1](#).

9. Kojima, T. (2004). The mechanism of *Drosophila* leg development along the proximodistal axis. *Dev. Growth Differ.* 46, 115–129.
10. Prpic, N.-M., and Telford, M.J. (2008). Expression of *homothorax* and *extradenticle* mRNA in the legs of the crustacean *Parhyale hawaiensis*: evidence for a reversal of gene expression regulation in the pancrustacean lineage. *Dev. Genes Evol.* 218, 333–339.
11. Williams, T., Nulsen, C., and Nagy, L.M. (2002). A complex role for *distal-less* in crustacean appendage development. *Dev. Biol.* 241, 302–312.
12. Hughes, C.L., and Kaufman, T.C. (2002). Hox genes and the evolution of the arthropod body plan. *Evol. Dev.* 4, 459–499.
13. Pearson, J.C., Lemons, D., and McGinnis, W. (2005). Modulating Hox gene functions during animal body patterning. *Nat. Rev. Genet.* 6, 893–904.
14. Abzhanov, A., and Kaufman, T.C. (1999). Novel regulation of the homeotic gene *Scr* associated with a crustacean leg-to-maxilliped appendage transformation. *Development* 126, 1121–1128.
15. Abzhanov, A., and Kaufman, T.C. (1999). Homeotic genes and the arthropod head: expression patterns of the *labial*, *proboscipedia*, and *Deformed* genes in crustaceans and insects. *Proc. Natl. Acad. Sci. USA* 96, 10224–10229.
16. Abzhanov, A., and Kaufman, T.C. (2000). Crustacean (malacostracan) Hox genes and the evolution of the arthropod trunk. *Development* 127, 2239–2249.
17. Abzhanov, A., and Kaufman, T.C. (2000). Embryonic expression patterns of the Hox genes of the crayfish *Procambarus clarkii* (Crustacea, Decapoda). *Evol. Dev.* 2, 271–283.
18. Averof, M., and Patel, N.H. (1997). Crustacean appendage evolution associated with changes in Hox gene expression. *Nature* 388, 682–686.
19. Deutsch, J.S., and Mouchel-Vielh, E. (2003). Hox genes and the crustacean body plan. *BioEssays* 25, 878–887.
20. Schram, F.R., and Koenemann, S. (2001). Developmental genetics and arthropod evolution: part 1, on legs. *Evol. Dev.* 3, 343–354.
21. Liubicich, D.M., Serano, J.M., Pavlopoulos, A., Kontarakis, Z., Protas, M.E., Kwan, E., Chatterjee, S., Tran, K.D., Averof, M., and Patel, N.H. (2009). Knockdown of *Parhyale* Ultrabithorax recapitulates evolutionary changes in crustacean appendage morphology. *Proc. Natl. Acad. Sci. USA* 106, 13892–13896.
22. Pavlopoulos, A., Kontarakis, Z., Liubicich, D.M., Serano, J.M., Akam, M., Patel, N.H., and Averof, M. (2009). Probing the evolution of appendage specialization by Hox gene misexpression in an emerging model crustacean. *Proc. Natl. Acad. Sci. USA* 106, 13897–13902.
23. Kato, Y., Shiga, Y., Kobayashi, K., Tokishita, S., Yamagata, H., Iguchi, T., and Watanabe, H. (2011). Development of an RNA interference method in the cladoceran crustacean *Daphnia magna*. *Dev. Genes Evol.* 220, 337–345.
24. Copf, T., Rabet, N., and Averof, M. (2006). Knockdown of spalt function by RNAi causes de-repression of Hox genes and homeotic transformations in the crustacean *Artemia franciscana*. *Dev. Biol.* 298, 87–94.
25. Gerberding, M., Browne, W.E., and Patel, N.H. (2002). Cell lineage analysis of the amphipod crustacean *Parhyale hawaiensis* reveals an early restriction of cell fates. *Development* 129, 5789–5801.
26. Lee, Y.S., and Carthew, R.W. (2003). Making a better RNAi vector for *Drosophila*: use of intron spacers. *Methods* 30, 322–329.
27. Angelini, D.R., and Kaufman, T.C. (2005). Functional analyses in the milkweed bug *Oncopeltus fasciatus* (Hemiptera) support a role for Wnt signaling in body segmentation but not appendage development. *Dev. Biol.* 283, 409–423.
28. Brown, S.J., Shippy, T.D., Beeman, R.W., and Denell, R.E. (2002). *Tribolium* Hox genes repress antennal development in the gnathos and trunk. *Mol. Phylogenet. Evol.* 24, 384–387.
29. DeCamillis, M.A., Lewis, D.L., Brown, S.J., Beeman, R.W., and Denell, R.E. (2001). Interactions of the *Tribolium* *Sex combs reduced* and *proboscipedia* orthologs in embryonic labial development. *Genetics* 159, 1643–1648.
30. Hrycaj, S., Chesebro, J., and Popadić, A. (2010). Functional analysis of *Scr* during embryonic and post-embryonic development in the cockroach, *Periplaneta americana*. *Dev. Biol.* 341, 324–334.
31. Smith, F.W., and Jockusch, E.L. (2014). Hox genes require homothorax and extradenticle for body wall identity specification but not for appendage identity specification during metamorphosis of *Tribolium castaneum*. *Dev. Biol.* 395, 182–197.
32. Gilles, A.F., and Averof, M. (2014). Functional genetics for all: engineered nucleases, CRISPR and the gene editing revolution. *Evodevo* 5, 43.
33. Spears, T., DeBry, R.W., Abele, L.G., Chodyla, K., and Boyko, C.B. (2005). Peracardid monophly and interordinal phylogeny inferred from nuclear small-subunit ribosomal DNA sequences (Crustacea: Malacostraca: Peracarida). *Proc. Biol. Soc. Wash.* 118, 117–157.
34. Yen, S.-T., Zhang, M., Deng, J.M., Usman, S.J., Smith, C.N., Parker-Thornburg, J., Swinton, P.G., Martin, J.F., and Behringer, R.R. (2014). Somatic mosaicism and allele complexity induced by CRISPR/Cas9 RNA injections in mouse zygotes. *Dev. Biol.* 393, 3–9.
35. Nakanishi, T., Kato, Y., Matsuura, T., and Watanabe, H. (2014). CRISPR/Cas-mediated targeted mutagenesis in *Daphnia magna*. *PLoS ONE* 9, e98363.
36. Shiga, Y., Sagawa, K., Takai, R., Sakaguchi, H., Yamagata, H., and Hayashi, S. (2006). Transcriptional readthrough of Hox genes *Ubx* and *Antp* and their divergent post-transcriptional control during crustacean evolution. *Evol. Dev.* 8, 407–414.
37. Averof, M., and Akam, M. (1995). Hox genes and the diversification of insect and crustacean body plans. *Nature* 376, 420–423.
38. Kelsh, R., Weinzierl, R.O., White, R.A., and Akam, M. (1994). Homeotic gene expression in the locust *Schistocerca*: an antibody that detects conserved epitopes in Ultrabithorax and abdominal-A proteins. *Dev. Genet.* 15, 19–31.
39. Durston, A.J. (2012). Global posterior prevalence is unique to vertebrates: a dance to the music of time? *Dev. Dyn.* 241, 1799–1807.
40. Akam, M. (1998). Hox genes, homeosis and the evolution of segment identity: no need for hopeless monsters. *Int. J. Dev. Biol.* 42, 445–451.
41. Averof, M., Pavlopoulos, A., and Kontarakis, Z. (2010). Evolution of new appendage types by gradual changes in Hox gene expression – the case of crustacean maxillipeds. *Paleodiversity* 3, 141–145.
42. Abzhanov, A., Holtzman, S., and Kaufman, T.C. (2001). The *Drosophila* proboscis is specified by two Hox genes, *proboscipedia* and *Sex combs reduced*, via repression of leg and antennal appendage genes. *Development* 128, 2803–2814.
43. Angelini, D.R., and Kaufman, T.C. (2004). Functional analyses in the hemipteran *Oncopeltus fasciatus* reveal conserved and derived aspects of appendage patterning in insects. *Dev. Biol.* 271, 306–321.
44. Ebner, A., Cabernard, C., Affolter, M., and Merabet, S. (2005). Recognition of distinct target sites by a unique Labial/Extradenticle/Homothorax complex. *Development* 132, 1591–1600.
45. Mann, R.S., Lelli, K.M., and Joshi, R. (2009). Hox Specificity: Unique Roles for Cofactors and Collaborators. In *Current Topics in Developmental Biology, Chapter 3*, O. Pourquié, ed. (Academic Press), pp. 63–101.
46. Merabet, S., and Hudry, B. (2013). Hox transcriptional specificity despite a single class of cofactors: are flexible interaction modes the key? Plasticity in Hox/PBC interaction modes as a common molecular strategy for shaping Hox transcriptional activities. *BioEssays* 35, 88–92.
47. Mito, T., Ronco, M., Uda, T., Nakamura, T., Ohuchi, H., and Noji, S. (2008). Divergent and conserved roles of extradenticle in body segmentation and appendage formation, respectively, in the cricket *Gryllus bimaculatus*. *Dev. Biol.* 313, 67–79.
48. Rivas, M.L., Espinosa-Vázquez, J.M., Sambrani, N., Greig, S., Merabet, S., Graba, Y., and Hombriá, J.C. (2013). Antagonism versus cooperativity with TALE cofactors at the base of the functional diversification of Hox protein function. *PLoS Genet.* 9, e1003252.

49. Ronco, M., Uda, T., Mito, T., Minelli, A., Noji, S., and Klingler, M. (2008). Antenna and all gnathal appendages are similarly transformed by homo-thorax knock-down in the cricket *Gryllus bimaculatus*. *Dev. Biol.* 313, 80–92.
50. Sambrani, N., Hudry, B., Maurel-Zaffran, C., Zouaz, A., Mishra, R., Merabet, S., and Graba, Y. (2013). Distinct molecular strategies for Hox-mediated limb suppression in *Drosophila*: from cooperativity to dispensability/antagonism in TALE partnership. *PLoS Genet.* 9, e1003307.
51. Slattery, M., Riley, T., Liu, P., Abe, N., Gomez-Alcalá, P., Dror, I., Zhou, T., Rohs, R., Honig, B., Bussemaker, H.J., and Mann, R.S. (2011). Cofactor binding evokes latent differences in DNA binding specificity between Hox proteins. *Cell* 147, 1270–1282.
52. Bassett, A., and Liu, J.-L. (2014). CRISPR/Cas9 mediated genome engineering in *Drosophila*. *Methods* 69, 128–136.
53. Blitz, I.L., Biesinger, J., Xie, X., and Cho, K.W.Y. (2013). Biallelic genome modification in F(0) *Xenopus tropicalis* embryos using the CRISPR/Cas system. *Genesis* 51, 827–834.
54. Hwang, W.Y., Fu, Y., Reyon, D., Maeder, M.L., Tsai, S.Q., Sander, J.D., Peterson, R.T., Yeh, J.-R.J., and Joung, J.K. (2013). Efficient genome editing in zebrafish using a CRISPR-Cas system. *Nat. Biotechnol.* 31, 227–229.
55. Kontarakis, Z., and Pavlopoulos, A. (2014). Transgenesis in Non-model Organisms: The Case of *Parhyale*. In *Hox Genes, Methods in Molecular Biology*, Y. Graba, and R. Rezsöhazy, eds. (Springer), pp. 145–181.
56. Pavlopoulos, A., and Averof, M. (2005). Establishing genetic transformation for comparative developmental studies in the crustacean *Parhyale hawaiensis*. *Proc. Natl. Acad. Sci. USA* 102, 7888–7893.
57. Rehm, E.J., Hannibal, R.L., Chaw, R.C., Vargas-Vila, M.A., and Patel, N.H. (2009). Injection of *Parhyale hawaiensis* blastomeres with fluorescently labeled tracers. *Cold Spring Harb. Protoc.* 2009, pdb.prot5128.